Sensors and Materials, Vol. 35, No. 8 (2023) 2947–2960
MYU Tokyo

S & M 3366

Enhanced Acetone Gas Sensing Using CuO Nanowires Embedded with Au Nanoparticles

Zihao Wang, Boyun Liu,* Shengnan Li, and Qi Shu

Graduate School, Department of Power Engineering, Naval Engineering University, Wuhan 430000, China

(Received April 19, 2023; accepted June 26, 2023)

Keywords: CuO nanowires, Au-functionalized CuO nanowires, acetone gas sensors, high response rate, ultrafast response/recovery time

The development of efficient acetone gas sensors is essential for the real-time monitoring of acetone gases in the environment. Here, CuO nanowires embedded with Au nanoparticles (NPs) with defined size, structure, and physicochemical properties are fabricated by a wet chemical method and are found to show enhanced acetone gas sensing behavior. The precise and controllable loading of Au NPs in CuO nanowires plays a critical role in modulating the acetone gas sensing behavior. The Au/CuO-nanowire-based sensors exhibit higher response rate, faster response/recovery, and better long-term stability than the pure CuO nanowires owing to the decrease in the width of the hole accumulation layer (HAL), larger specific surface area, and more active sites for gas diffusion. Our present work may have potential application in the real-time monitoring of gases in an actual environment owing to its high response rate, ultrafast response/recovery time and long-term stability.

1. Introduction

Metal oxide semiconductors (MOSs) have been widely investigated as gas sensors.[1,2] To the best of our knowledge, in most studies, MOS-based gas sensors usually involve n-type materials such as ZnO, Fe_2O_3, and SnO_2.[3–5] According to the theory of semiconductors, these n-type semiconductors form electron-depletion layers upon the adsorption of molecules on their surfaces, which leads to changes in conductivity. Nanoscale materials have a larger surface area than normal materials, so they are known to have superior functional properties than larger pieces of material, which contribute to a stronger reaction with the detection gas.[6] In recent studies, 1D materials such as nanowires and nanoribbons are usually considered as sensitive materials and applied to specific gas sensors.[7]

However, the performance of gas sensors still needs to be improved in scientific research and practical applications, so a number of approaches have been employed. A common approach is to build p-n junctions with other types of MOS decoration to improve the sensing performance.

*Corresponding author: e-mail: 1029800013@qq.com
https://doi.org/10.18494/SAM4434

ISSN 0914-4935 © MYU K.K.
https://myukk.org/

Because the p-n heterostructure interface can provide electrical junction properties, the electron and hole carriers of two types of semiconductor material can be changed.[8]

Another modification of nanoscale semiconductor materials is to build metal–semiconductor junctions by decorating the surface of MOS with metal nanoparticles (NPs), such as noble metal elements (gold, platinum, palladium, etc.).[9] Noble metal NPs have outstanding catalytic activity and can accelerate the reaction between the target gas and oxygen molecules; moreover, many studies have shown that noble metals can promote the chemisorption of molecular oxygen and molecular gases.[10] Regarding other phenomena, the formation of ohmic contacts and Schottky barriers at the oxide/metal interface will lead to more free electron flow from noble metals to oxides; Fermi-level variations between bare oxide and oxide/metal heterostructures and different work functions of oxide and metal materials will suppress electron–hole complexation; and having more free electrons will also contribute to improving the sensing performance of semiconductor-based gas sensors.

Among MOSs, Cu(II) oxides have significant application potential, and recently, CuO with diverse structures have been fabricated as typical p-type semiconductors, and their sensing properties have been extensively studied to evaluate their practical applications in sensor devices. In addition, p-type CuO has emerged as a material with great promise in addition to the conventional n-type materials because nanoscale CuO shows superb surface reactivity, unique electrical properties, and inherent catalytic activity.[11]

On the basis of the above considerations, we report a convenient, environment-friendly, and cost-effective route to fabricate CuO nanowires functionalized with Au NPs. The prepared Au/CuO system was used for detecting acetone gas and showed a high response rate and a short response/recovery time even at low operating temperatures, and the sensing performance depends on the amount of Au NPs. The gas sensor properties of CuO nanowires were significantly improved by decorating Au NPs. In particular, the development of Au/CuO can provide an interesting perspective to explain the sensing mechanism.

2. Experimental Procedure

The reagents were of analytical grade and used without further purification.

2.1 Synthesis of Au/CuO nanowires

CuO nanowires ($20 \times 20 \times 0.15$ mm^3) on copper foil were prepared by the method described in our previous report.[12] In a typical synthesis experiment, CuO nanowires decorated with Au NPs were synthesized by a wet chemical method. First, the prepared CuO nanowires were immersed in a 40 mL ethanol solution containing 0.05 g of $SnCl_2$ and stirred vigorously at room temperature for about 30 min to obtain activated CuO nanowires. Subsequently, the activated CuO nanowires were immersed in a 50 mL ethanol solution containing 1.0 ml of 0.01 g/ml $HAuCl_4$ solution and stirred for about 2 h. Then, the products were removed, rinsed, and dried. Finally, the products were annealed at 300 °C for 6 h. In the synthesis experiments, we varied the amount of $HAuCl_4$ to control the number of Au NPs on the surface of CuO nanowires. Figure 1 shows a schematic of the fabrication of Au-functionalized CuO nanowires.

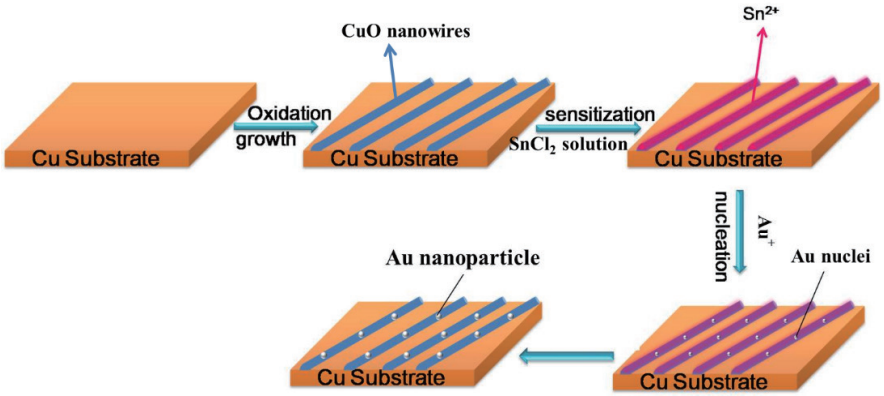

Fig. 1. (Color online) Schematic of the fabrication of CuO nanowires functionalized with Au NPs.

2.2 Characterization and gas-sensing measurements

X-ray diffraction (XRD) measurements were performed on a Dmax-3b diffractometer using nickel-filtered Cu Ka radiation (k = 1.54178 A). The morphology of the products was studied by field emission scanning electron microscopy (FESEM; JEOL-6300 F). X-ray photoelectron spectroscopy (XPS) spectra were collected using an ESCA Lab MKII X-ray photoelectron spectrometer (KAlpha 1063).

Gas sensing characteristics were detected using the Navigation 4000-NMDOG gas sensing measurement instrument, which is schematically shown in Fig. 2. The concentration of the target gas obtained from the liquid is calculated using

$$C = \frac{22.4 \times \varnothing \times \rho \times V_1}{M \times V_2},$$

where C (ppm) is the concentration of the target gas, Ø is the desired gas volume fraction, ρ (g/mL) is the density of the liquid, V_1 (μL) is the volume of the liquid, V_2 (L) is the volume of the chamber, and M (g/mol) is the molecular weight of the liquid.

For reducing gases, the sensor response is defined as $S = R_g/R_a$, where R_a and R_g are the resistances of the gas sensor in clean air and in the target gas, respectively. In addition, the response time τres is defined as the time required for the initial value to reach 90% of the stable value, whereas the recovery time τrec is defined as the time required for the stable value to decrease by 90% when the gas sensor is removed from the target gas into air.

3. Results and Discussion

3.1 Structural and morphological characteristics

The structural phases of CuO nanowires functionalized with Au were investigated by XRD. Figure 3 shows typical XRD patterns of CuO nanowires functionalized with Au NPs of different

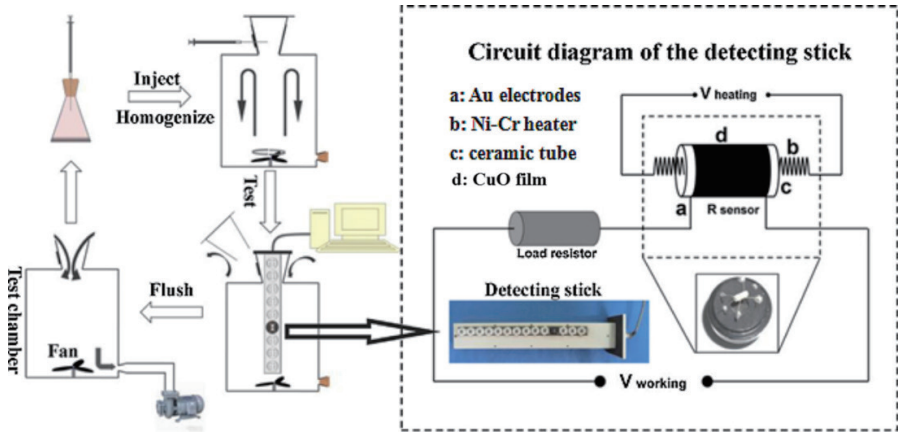

Fig. 2. (Color online) Schematic of gas sensing measurement system.

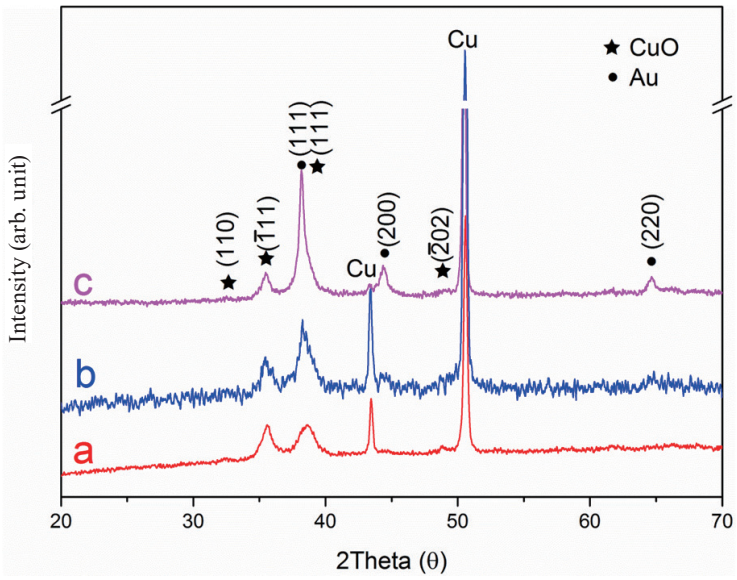

Fig. 3. (Color online) Typical XRD patterns of CuO nanoribbons with different contents of Au NPs: (a) 0.8, (b) 1.0, and (c) 1.5 ml.

contents. The pattern obtained matches well with that of the monoclinic CuO phase (JCPDS No. 41-0254), except for the peaks of the copper foil. The presence of the Au diffraction peak (JCPDS No. 04-0784) confirms the formation of Au NPs on CuO nanowires. It is clear that the intensity of the Au peak increases with increasing content of Au NPs, most likely owing to the higher number of Au NPs on the CuO nanowires.

SEM was used to study the microstructure and surface morphology of CuO nanowires with Au NPs. As shown in Fig. 4, the CuO nanowires are almost perpendicular to the substrate surface with a length of about 2 μm and a width of about 100 nm. Different amounts of Au NPs

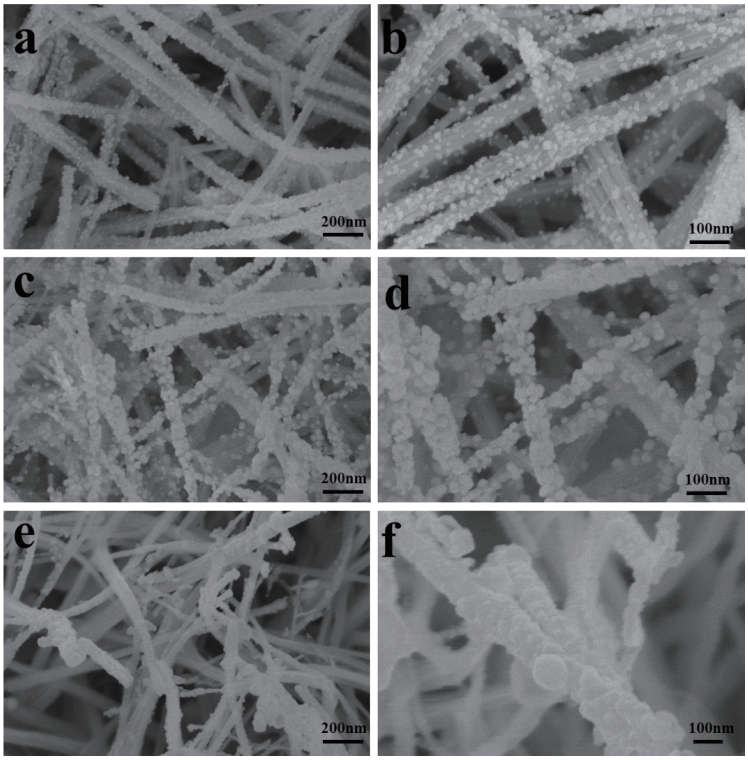

Fig. 4. Microstructures of CuO nanoribbons functionalized with different contents of Au NPs: (a) and (b) 0.8, (c) and (d) 1.0, and (e) and (f) 1.5 ml.

were attached to the CuO nanowires. Spherical metallic Au NPs were encapsulated on the surface of the CuO nanowires with sizes ranging from 40 to 60 nm. As the amount of $HAuCl_4$ solution was increased and the reaction time was lengthened, more Au NPs appeared and their sizes changed. In general, the morphology and crystallinity of the original CuO nanowires were preserved during Au deposition owing to the mild wet chemical conditions used. Importantly, the amount of Au NPs increased with increasing amount of $HAuCl_4$. Figure 4 shows the relationship between the amounts of NP and $HAuCl_4$. A larger amount of $HAuCl_4$ may provide more new Au nuclei on the surface of CuO nanowires, which would easily form more Au NPs.

The surface composition of the obtained systems was analyzed by XPS, and Fig. 5(a) shows the XPS spectra of the Au-functionalized CuO nanowires. Figures 5(b)–5(d) show the high-resolution XPS spectra of Cu, Au, and O, respectively. The two peaks located at 932.98 and 952.78 eV are designated as $Cu2p_{3/2}$ and $Cu2p_{1/2}$, respectively [see Fig. 5(b)]. These values are in good agreement with the reported results for Cu2p in CuO.[13,14] Meanwhile, the gap between the two Cu levels is 19.8 eV, which is in good agreement with the standard spectrum of Cu. In addition, the presence of two dithered satellites at the higher binding energies of 940.38 and 943.18 eV for the Cu2p peak confirms the oxidation state of Cu (II).[15] The O1s core level spectrum, decomposed by the Gaussian method into three peaks at 529.9 and 531.5 eV, is designated as O^{2-} for lattice oxygen, OH^- or O^- for surface adsorbed oxygen, and O^{2-} for surface

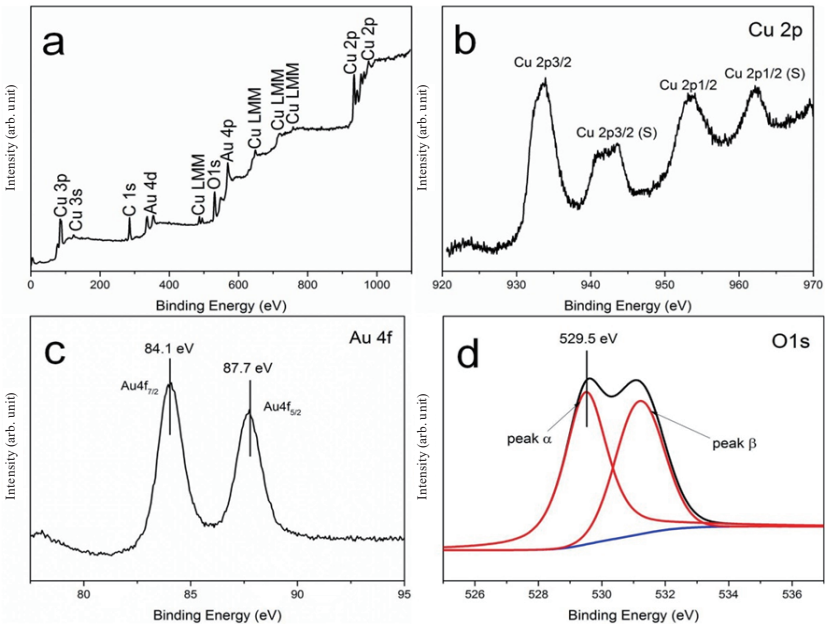

Fig. 5. (Color online) (a) Wide XPS spectrum of Au-functionalized CuO nanoribbons, and high-resolution XPS spectra of (b) Cu2p, (c) Au4f, and (d) O1s.

chemisorbed oxygen.[16] Regarding Au, peaks at about 84.1 and 87.7 eV are assigned to $Auf_{7/2}$ and $Auf_{5/2}$, respectively, which are higher than the peaks usually detected for metallic Au, which may be due to the formation of a Schottky junction at the Au/CuO interface, resulting in the flow of electrons from the metal to the vacant state in the MOS valence band. In fact, the gas sensing data also support this.

3.2 Gas sensing properties

The operating temperature is considered to be an important factor that considerably affects the gas reaction. We investigated the responses of four sensors based on pure CuO nanowires and CuO nanowires with different contents of Au NPs, and thus measured the responses of the sensors exposed to 50 ppm acetone over the operating temperature range from 25 to 240 °C. Figure 6 clearly shows the results of the temperature-dependent response measurements. We can clearly see that the response of the sensor based on pure CuO nanowires to acetone increases with increasing temperature, but those of the sensors based on Au/CuO nanowires increase with increasing temperature up to a certain point and then decrease rapidly.

Moreover, the maximum response values of the pure CuO-nanowire-based sensors were obtained at 240 °C, and the maximum response values of Au/CuO-nanowire-based sensors were obtained at 180 °C. The response value of the sensor based on CuO nanowires with Au NPs (1.0 ml) was up to 16.5, which is five times higher than that of the gas sensor based on CuO nanowires. Apparently, after functionalization with Au NPs, the response of the CuO-nanowire-

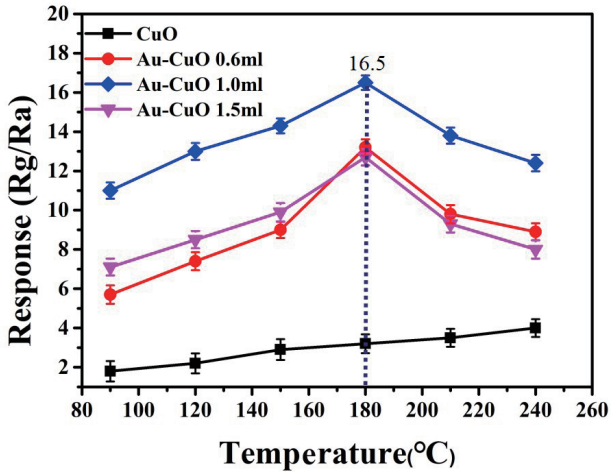

Fig. 6. (Color online) Variations of response (R_g/R_a) of four sensors exposed to 50 ppm acetone at different operating temperatures.

based sensor was significantly improved and the optimal operating temperature was lower. Moreover, the response decreased with increasing temperature after the appearance of the optimum operating temperature. This could mean that very high temperatures are not favorable for absorbing gas molecules. When we used a 1.0 ml dose of $HAuCl_4$ to functionalize the CuO nanowires, the response to acetone gas showed the maximum. This response behavior suggests that when Au NPs are used for the functionalization of oxides, the amount of Au NPs must be optimized to obtain excellent sensing performance.

The dynamic response characteristics of the sensors exposed to acetone were investigated. Figures 7(a) and 7(b) show the reproducibility of the responses of the sensors exposed to ambient atmosphere, which was cycled between clean air and air with 50 ppm acetone. The response of the Au/CuO-nanowire-based sensors was reproducible and did not vary significantly over the four cycles of testing, and in particular, these sensors showed a higher response rate, which has great potential for practical applications. The response/recovery times to 50 ppm acetone are shown in Figs. 7(c) and 7(d), respectively. The response/recovery times of CuO nanowires and Au/CuO nanowires exposed to 50 ppm acetone are 30 /35 s and 1.2 /12 s, respectively. The Au/CuO-nanowire-based sensor has an ultrafast response/recovery time. The Au/CuO nanowires exhibit superior gas sensing characteristics compared with various morphological gas sensors described in previous reports, which are listed in Table 1.[17–23]

Figure 8(a) shows the response curves of the sensors exposed to 10 to 500 ppm acetone gas. The sensor responses all become higher as the acetone concentration increases. Furthermore, the sensors based on CuO nanowire and Au/CuO nanowire exhibit good linearity with respect to the concentration. Notably, the response of the Au/CuO-nanowire-based sensors was significantly higher than that of the CuO-nanowire-based sensors. Even at low concentrations, such as 10 ppm, the sensors based on CuO nanowires functionalized with Au NPs exhibit a good response and can be used to detect low concentrations of the target gas. As for the device, the long-term characteristics are also important. Figure 8(b) shows the long-term stability of the sensor. In 56 days of measurements, the response of the CuO-nanowire-based sensor decreased

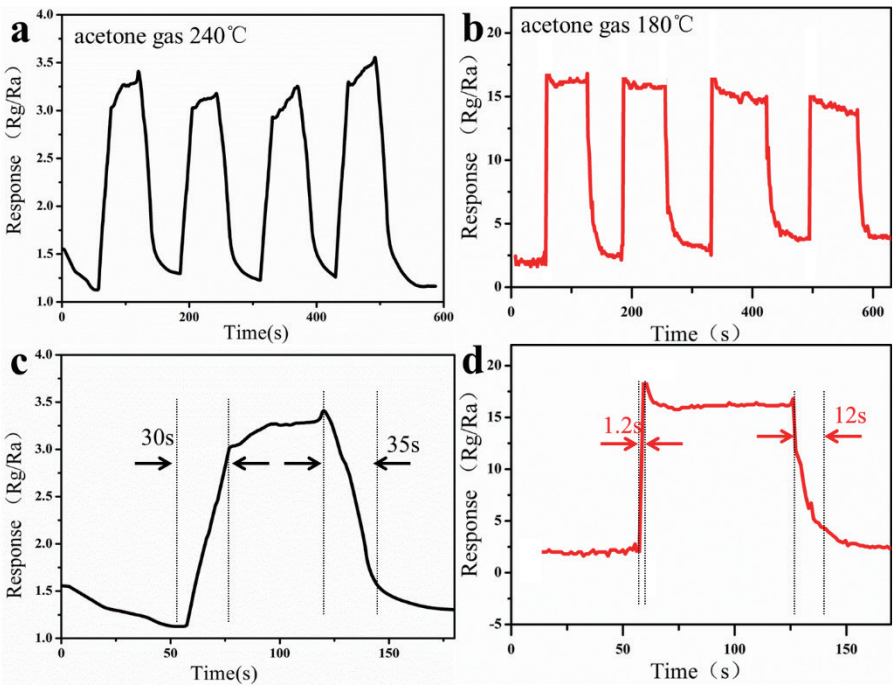

Fig. 7. (Color online) (a) Response and recovery time measurements (four cycles) of the pure CuO-nanowire-based sensors exposed to 50 ppm acetone gas at 240 °C. (b) Response and recovery time measurements (four cycles) of the Au/CuO-nanowire-based sensors exposed to 50 ppm acetone gas at 180 °C. (c) Response and recovery time measurements (one cycle) of the pure CuO-nanowire-based sensors exposed to 50 ppm acetone gas at 240 °C. (d) Response and recovery time measurements (one cycle) of the Au/CuO-nanowire-based sensors exposed to 50 ppm acetone gas at 180 °C.

Table 1
Gas sensing characteristics of MOS-based gas sensors reported so far and in current work.

Materials	Gas	Concentration (ppm)	Temperature (°C)	Response	τ_{res}/τ_{rec} time (s)	Reference
CuO nanorods	H_2	50	200	4.7	—	Ref. 17
CuO nanowires	C_4H_9OH	50	350	5.2	22/53	Ref. 18
CuO nanodisks	C_2H_5OH	100	300	6.2	119/35	Ref. 19
CuO/$ZnSnO_3$ hollow microspheres	C_2H_5OH	10	160	22	13/8	Ref. 20
CuO/SnO_2	H_2S	10	140	2.0	94/114	Ref. 21
$CuFe_2O_4$/CuO microspheres	H_2S	10	240	23	31/40	Ref. 22
CuO/Ga_2O_3 thin films	C_3H_6O	1.25	300	1.3	187/525	Ref. 23
CuO nanocubes		0.8	300	1.17	—	Ref. 24
ZnO-CuO core-hollow cube nanostructures		1	200	11.14	—	Ref. 25
Au/CuO nanowires	C_3H_6O	50	180	16.5	1.2/12	This work

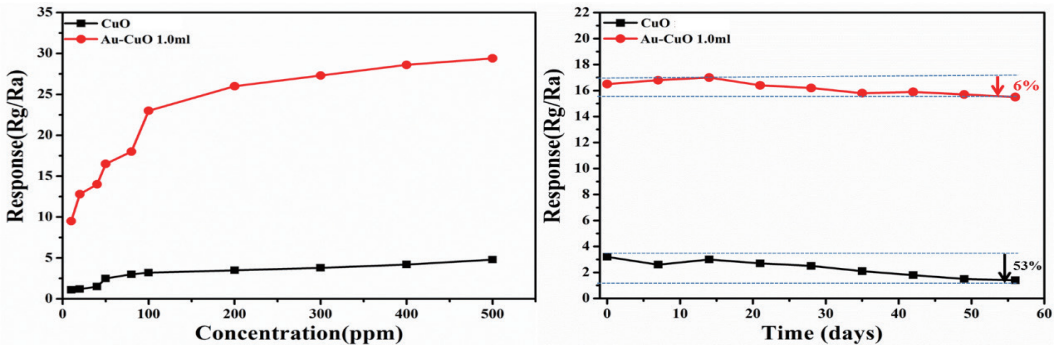

(a) (b)

Fig. 8. (Color online) (a) Response curves of the two sensors based on CuO and Au–CuO exposed to 10 to 500 ppm acetone gas. (b) Long-term stability of the two sensors based on CuO and Au-CuO nanowires.

significantly (53%), but at the same time, that of the Au/CuO-nanowire-based sensor decreased by only 6%, which is favorable for the detection of acetone gas in real life.

Indeed, the gas environment is complex and high selectivity is very important. Thus, we detected several different target gases (acetone, methanol, ethanol, ammonia, and formaldehyde) at a concentration of 50 ppm, and the results are shown in Fig. 9. We can see that after functionalization with Au NPs, the Au/CuO-nanowire-based sensor shows higher gap sensitivity to acetone than to the other target gases compared with the bare CuO.

We also added 50 ppm of interfering gas at the ambient temperature to 180 °C and the acetone gas to 50 ppm and then checked for changes in the reaction. As shown in the responses given in Table 2, the interfering gas has little effect on the response of the Au/CuO-nanowire-based gas sensor, further demonstrating the good selectivity and interference resistance of this sensor.

In general, gas sensing is a surface-related mechanism based on the change in resistance of the sensor upon the adsorption and desorption of gas molecules. Although p-type oxides have been much less studied than n-type systems, they have recently attracted significant interest in gas sensing applications owing to their unique catalytic activity, surface reactivity, and electrical properties. When p-type oxides are exposed to air, oxygen molecules adsorb to their surfaces and ionize into species such as O_2^-, O^-, and O^{2-} by collecting electrons from the semiconductor surface [Eqs. (1)–(4)].

$$O_2(\text{gas}) \rightarrow O_2(\text{ads}) \tag{1}$$

$$O_2(\text{ads}) + e^- \rightarrow O_2^-(\text{ads}) \tag{2}$$

$$O_2^-(\text{ads}) + e^- \rightarrow 2O^-(\text{ads}) \tag{3}$$

$$O^-(\text{ads}) + e^- \rightarrow O^{2-}(\text{ads}) \tag{4}$$

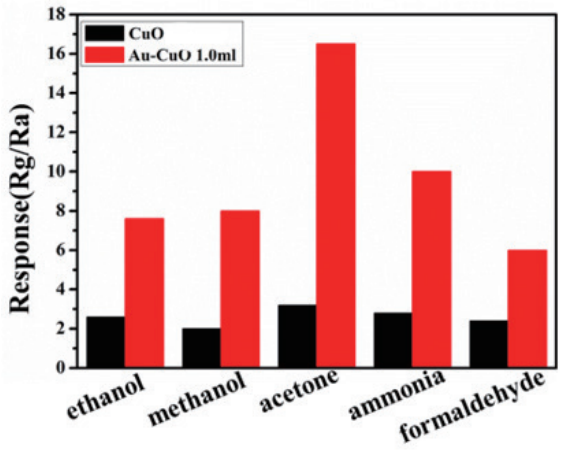

Fig. 9. (Color online) Selectivity test results of the two sensors based on CuO and Au/CuO (1.0 ml) nanowires exposed to various gases at 50 ppm and 180 °C.

Table 2
Variations in response (R_g/R_a) of two sensors exposed to different interfering gases at 50 ppm.

Target gas (50 ppm)	Response	
	CuO nanowires	Au/CuO nanowires
acetone	3.5	16.5
acetone + ethanol	4.5	17
acetone + ethanol + ammonia	6	18.5
acetone + ethanol + methanol+ ammonia	6.5	18

The establishment of the hole accumulation layer (HAL) is caused by an increase in the concentration of holes near the surface; this can be described by an energy band representation as an upward band bend where the resistance of the gas sensor will decrease (Fig. 10).

When the p-type system is exposed to the acetone gas, acting as an electron-trapping adsorbate, the following reactions take place (Fig. 10).

$$CH_3COCH_3 + 8O^-(ads) \rightarrow 3CO_2 + 3H_2O + 8e^- \quad (5)$$

$$CH_3COCH_3 + 8O^{2-}(ads) \rightarrow 3CO_2 + 3H_2O + 16e^- \quad (6)$$

$$e^-(ads) + h^+ \rightarrow Null \quad (7)$$

As a result, the HAL width (or hole concentration) decreases further and the measured sensor resistance is higher than the original air value [Figs. 11(a)–11(c)].

In this case, the performance of the Au/CuO-nanowire-based sensor is significantly enhanced, which can be attributed to electronic and chemical sensitization. Concerning electronic sensitization, the formation of a Schottky junction at the Au/CuO interface will result

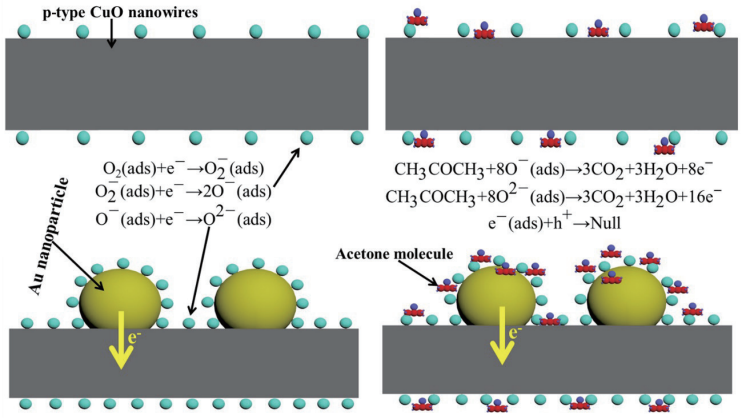

Fig. 10. (Color online) Schematic of acetone sensing mechanisms of Au/CuO nanowires.

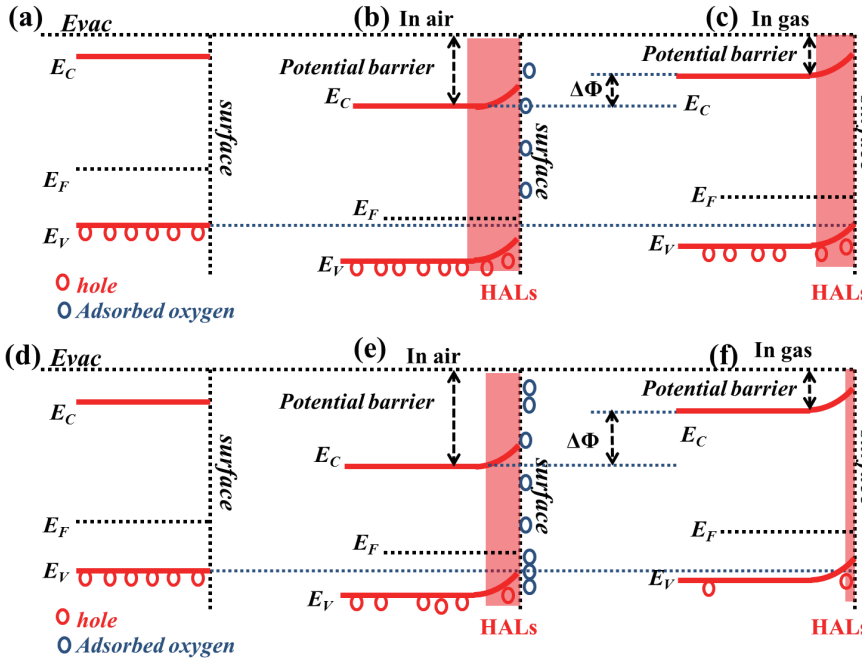

Fig. 11. (Color online) Schematic of HAL thickness modulation for (a)–(c) bare CuO nanowires and (d)–(f) Au-CuO nanowires.

in the flow of electrons from the metal Au to p-type CuO. The occurrence of this phenomenon is also supported by the present XPS data in comparison with CuO, and is expected to reduce the width of the HAL conduction channel in the Au/CuO specimen, as actually observed [Figs. 10 and 11(e)]. More free electrons flowing from metallic Au to the p-type CuO surface can simultaneously cause more chemisorbed oxygen molecules to adsorb on the CuO surface and react with acetone gas molecules (Fig. 10). Apparently, these reactions [Eqs. (1)–(7)] are more intense than those of bare CuO, which leads to a sharp decrease in the thickness of the Au/CuO

nanowire HALs and a sharp increase in the resistance of the gas sensor [Fig. 11(f)]. As to the response = R_g/R_a, the value of Rg/R_a is much smaller than that of bare CuO, so the response is improved. Concerning the chemical sensitization, the introduction of Au NPs can catalyze the promotion of the dissociation of molecular oxygen, whose atomic products then diffuse into the metal oxide support. In addition, Au NPs can accelerate the reaction between molecular oxygen and acetone gas, thus reducing the response/recovery time. Moreover, as shown in Fig. 4, Au NPs have a larger surface area than CuO nanowires owing to their granular shape and very irregular surface morphology, which can lead to the enhanced adsorption of acetone gas, thus leading to a higher reaction rate and improved gas sensing performance.

4. Conclusions

In summary, we have developed an acetone gas sensor based on composite CuO nanowires embedded with AuNPs of defined size and interparticle distance. The precise and adjustable loading of the AuNPs in the composite sensor causes an enhanced acetone sensing performance, owing to the decrease in the width of the HAL, larger specific surface area, and more active sites for gas diffusion. These advanced properties make it possible to apply this composite nanostructure to a wide range of research areas, such as biochemical sensors, catalysis, and semiconductor devices.

Acknowledgments

We sincerely thank the National Natural Science Foundation of China (21201156) for financially supporting this research.

References

1 Z. Li, X. Liu, M. Zhou, S. Zhang, S. Cao, G. Lei, C. Lou, and J. Zhang: J. Hazard. Mater. **415** (2021) 125757. https://doi.org/10.1016/j.jhazmat.2021.125757
2 S. Mahajan and S. Jagtap: Appl. Mater. Today **18** (2020) 100483. https://doi.org/10.1016/j.apmt.2019.100483
3 W. Qin, W, Zhenyu. Y, H. Gao, R. Zhang, and F. Meng: Sens. Actuators, B **341** (2021) 130015. https://doi.org/10.1016/j.snb.2021.130015
4 C. Zhang, S. Zhang, Y. Yang, H. Yu, and X. Dong: Sens. Actuators, B **325** (2020) 128804. https://doi.org/10.1016/j.snb.2020.128804
5 T. He, W. Liu, T. Lv, M. Ma, Z. Liu, A. Vasiliev, and X. Li: Sens. Actuators, B **329** (2021) 129275. https://doi.org/10.1016/j.snb.2020.129275
6 S. H. Lu, Y. Z. Zhang, J. Y. Liu, H. Y. Li, Z. X. Hu, X. Luo, N. B. Gao, B. Zhang, J. J. Jiang, A. H. Zhong, J. T. Luo, and H. Liu: Sens. Actuators, B **345** (2021) 130334. https://doi.org/10.1016/j.snb.2021.130334
7 E. Salih and A. I. Ayesh: Mater. Chem. Phys. **267** (2021) 124695. https://doi.org/10.1016/j.matchemphys.2021.124695
8 S. Nie, D. Dastan, J. Li, W. D. Zhou, S. S. Wu, Y. W. Zhou, and X. T. Yin: J. Phys. Chem. Solids. **150** (2021) 109864. https://doi.org/10.1016/j.jpcs.2020.109864
9 Y. S. Xu, W. Zheng, X. H. Liu, L. Q. Zhang, L. L. Zheng, C. Yang, N. Pinna, and J. Zhang: Mater. Horiz. **7** (2020) 1519. https://doi.org/10.1039/d0mh00495b
10 H. Cui, P. F. Jia, and X. Y. Peng: Appl. Surf. Sci. **513** (2020) 145863. https://doi.org/10.1016/j.apsusc.2020.145863
11 N. Wang, W. Tao, X. Q. Gong, L. P. Zhao, T. S. Wang, L. J. Zhao, F. M. Liu, X. M. Liu, P. Sun, and G. Y. Lu: Sens. Actuators, B **362** (2022) 131803. https://doi.org/10.1016/j.snb.2022.131803

12 X. Q. Liu, Z. Li, Q. Zhang, F. Li, and T. Kong: Mater. Lett. **72** (2012) 49. https://doi.org/10.1016/j.matlet.2011.12.077
13 C. K. Xu, Y. K. Liu, G. D. Xu, and G. H. Wang: Mater. Res. Bull. **37** (2002) 2365. https://doi.org/10.1016/s0025-5408(02)00848-6
14 P. E. Sobol, A. J. Nelson, C. R. Schwerdtfeger, W. F. Stickle and J. F. Moulder:Surf. Sci. Spectra. **1** (1992) 393. https://avs.scitation.org/doi/10.1116/1.1247638
15 R. A. Zarate, F. Hevia, S. Fuentes, V. M. Fuenzalida, and A. Zuniga: J. Solid State Chem. **180** (2007) 1464. https://doi.org/10.1016/j.jssc.2007.01.040
16 T. H. Yang, L. D. Huang, Y. W. Harn, C. C. Lin, J. K. Chang, C. I. Wu, and J. M. Wu: Small. **9** (2013) 3169. https://doi.org/10.1002/smll.201300424
17 D. P. Volanti, A. A. Felix, M. O. Orlandi, G. Whitfield, D. J. Yang, E. Longo, H. L. Tuller, and J. A. Varela: Adv. Funct. Mater. **23** (2013) 1759. https://doi.org/10.1002/adfm.201202332
18 M. E. Mazhar, , G. Faglia, E. Comini, D. Zappa, C. Baratto, and G. Sberveglieri: Sens. Actuators, B **222** (2016) 1257. https://doi.org/10.1016/j.snb.2015.05.050
19 A. Umar, J. H. Lee, R. Kumar, and O. Al-Dossary: J. Nanosci. Nanotechnol. **17** (2017) 1455. https://doi.org/10.1166/jnn.2017.12727
20 S. W. Yu, X. H. Jia, J. Yang, S. Z. Wang, Y. Li, and H. J. Song: Mater. Lett. **291** (2021) 129531. https://doi.org/10.1016/j.matlet.2021.129531
21 A. I. Ayesh, A. A. Alyafei, R. S. Anjum, R. M. Mohamed, M. B. Abuharb, B. Salah, and M. El-Muraikhi: Appl. Phys. A **125** (2019) 550. https://doi.org/10.1007/s00339-019-2856-6
22 X. B. Hu, Z. G. Zhu, Z. H. Li, L. L. Xie, Y. H. Wu, and L. Y. Zheng: Sens. Actuators, B **264** (2018) 139. https://doi.org/10.1016/j.snb.2018.02.110
23 K. Dyndal, A. Zarzycki, W. Andrysiewicz, D. Grochala, K. Marszalek, and A. Rydosz: Sensors **20** (2020) 3142. https://doi.org/10.3390/s20113142
24 H yung Ju Park, Nak-Jin Choi, Hyuntae Kang, Moon Youn Jung, Jeong Won Park, Kang Hyun Park, and Dae-Sik Lee: Sens. Actuators, B **203** (2014) 282. https://doi.org/10.1016/j.snb.2014.06.118
25 Jae Eun Lee,, Chan Kyu Lim, Hyung Ju Park, Hyunjoon Song, Sung-Yool Choi, and Dae-Sik Lee: ACS Appl. Mater. Interfaces **12** (2020)31. https://doi.org/10.1021/acsami.0c08593

About the Authors

Zihao Wang received his B.S. degree from Wuhan Engineering University, China, in 2020. Since 2021, he has been attending the Chinese People's Liberation Army Naval Engineering University for his M.S. degree. His research interests are in MEMS and sensors. (1209800013@qq.com)

Boyun Liu received his B.S. degree from the Naval Engineering University, China, in 1999 and his M.S. and Ph.D. degrees from the Chinese People's Liberation Army Naval Engineering University, China, in 2002 and 2006, respectively. From 2006 to 2009, he was a lecturer at the Naval Engineering University, China. Since 2010, he has been an assistant professor at the same university. His research interests are in sensors and safety monitoring and control. (boyunliu@163.com)

Shengnan Li received her B.S. degree from Wuhan Engineering University, China, in 2019. Since 2022, she has been attending the Chinese People's Liberation Army Naval Engineering University for her M.S. degree. Her research interests are in MEMS, bioengineering, and sensors. (LSN8960@163.com)

Qi Shu received her B.S. degree from the City College of Wuhan University of Science and Technology, China, in 2019. Since 2022, she has been attending the Chinese People's Liberation Army Naval Engineering University for her M.S. degree. Her research interests are in MEMS and sensors. (1023709476@qq.com)